Journal of Materials Chemistry A

Accepted Manuscript

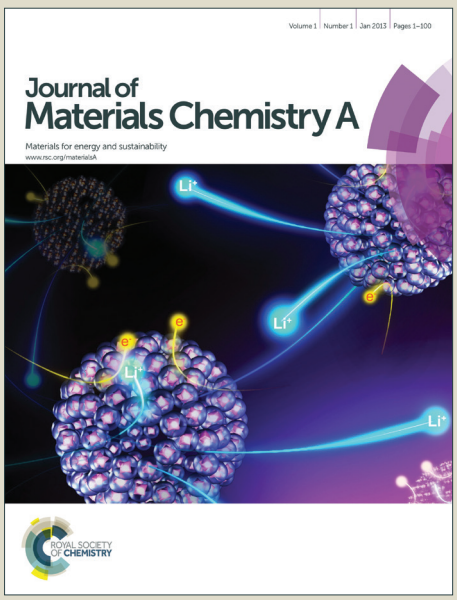

ROYAL SOCIETY OF CHEMISTRY

www.rsc.org/materialsA

Rate-dependent and Self-Healing Conductive Shear Stiffening Nanocomposite: A Novel Safe-guarding Material with Force Sensitivity

Sheng Wang[a,†], Shouhu Xuan[b,†], Wanquan Jiang[a*], Weifeng Jiang[b], Lixun Yan[b], Ya Mao[a], Mei Liu[a] and Xinglong Gong[b*]

[a]*Department of Chemistry, Collaborative Innovation Center of Suzhou Nano Science and Technology, University of Science and Technology of China (USTC), Hefei 230026, P. R. China*

[b]*CAS Key Laboratory of Mechanical Behavior and Design of Materials, Department of Modern Mechanics, USTC, Hefei 230027, P. R. China*

[*]*Corresponding author: Tel: 86-551-63607605; Fax: 86-551-63600419.*

E-mail: jiangwq@ustc.edu.cn (W.Q. Jiang)

gongxl@ustc.edu.cn (X.L. Gong)

[†]The two authors contributed equally to this work.

Abstract: A novel rate-dependent and self-healing conductive composite with well defined shear stiffening (ST) effect was facilely fabricated by dispersing the multi-walled carbon nanotube (MWCNT) into shear stiffening polymer matrix. The storage modulus (G') of the multifunctional composite automatically increased 4 orders of magnitude when encountering external shear stimuli and G'_{max} was over 1MPa, demonstrating an obvious shear stiffening effect and well safe-guarding performance. It was found that the electric conductivity changed accordingly when the shear stiffening happened, therefore it could be applied as a force sensor during the attacking. The rate-dependent piezoresistance effect of the composite was investigated. In quasi-static compression and high rate impact tests, different force signals could be obtained since the negative and positive piezoresistivity effect. Self-healing tests indicated the as-prepared composite can maintain its mechanical and electrical properties after destruction and healing treatment. Owing to the shear stiffening performance, the rate dependent conductive composite could both absorb impact energy and sense to the attacking forces. Finally, the mechanism was proposed and the glass transition induced by B-O interaction and the changes of microstructures during the external action were attributed to the ST performance and rate dependent electrical conductivity, respectively.

Keywords: Shear Stiffening Effect, MWCNT, Rate-dependent, Safe Guarding, Force Sensor.

1. Introduction.

In recent years, body armor has become a hot and challenge since large numbers of terrorisms, civil and international conflicts are rising in all the world. In the early stage, rigid materials such as metal[1,2] and ceramics[3,4] were applied to prepare body armors to resist against mechanical impact. However, the bulky, inflexible and uncomfortable drawbacks confined their widely application in the modern eras. Therefore, novel materials such as Kevlar fibers, high molecular weight polyethylene were developed for safeguards owing to their lightweight, flexibility, high Young's modulus and good performance against impact.[5-7] To date, the ballistic, puncture and stab performance of Kevlar fibers and high molecular weight polyethylene have been investigated and the protective helmets, body armor have been manufactured and applied in modern protective equipment. However, these materials only resist mechanical punch in a passive way and can not sense and response to the external force.

Flexible sensor, as a kind of electrically conductive polymer composite, can response external mechanical deformations and transduce the stimulus to electrical signals.[8-11] Commonly, they are composed of conductive fillers and flexible or stretchable polymer matrix.[12-15] Various piezoresistive,[16,17] capacitive,[18,19] and piezoelectric[20] force sensors have been developed in the past decades. Owing to their easy fabrication, high sensitivity, reliable stimuli-responsive properties and stretchability, force sensors have been applied in stretchable electronic devices,[21-23] wearable and implantable devices,[24] e-skins,[25] clinical practice and medical research. [26, 27]

Very recently, by introducing functional nanofillers or polymer matrix into force sensors, multifuntional stretchable force sensors have been achieved to meet the development of intelligent electronics. For example, novel e-skins were developed and they could sense heat, cold and discern pressures including human touch.[28, 29] Shan X.C. reported a tri-stimuli-responsive luminescent sensor which could detect temperature, mechanical force and solvent vapors.[9] Yao H.B. prepared a silver

nanowires-based wearable multifunctional sensors which could detect strain, pressure and finger touch with fast response time and high sensitivity.[30]

Shear thickening (ST) material is a kind of smart material whose viscosity can increase sharply once the applied stress is beyond a critical shear rate. Due to the sensitive rate dependent property, a number of attention has been paid to develop high performance ST materials. According to the composition and active mechanism, the ST materials can be classified into shear thickening fluid and shear stiffening polymer composite.[31, 32] Based on the unique mechanical properties, ST materials have been applied in vibration controlling, damping and body armor.[33-35] Recently, the shear stiffening polymer composite has been intensively studied since its potential application in safe garding areas. Tian T. F. studied the mechanical and rheological properties of shear-stiffened elastomer.[32] Based on the ST gel, Palmer R. developed a new kind of body armor which could absorb much energy during impact.[36] The conbination of ST with other functionalities together could give out novel high performance smart body armor. For example, multifunctional polymer composite with both excellent ST property and magnetorheological effect could be achieved by introducing mangetic particles into the ST matrix.[37] The increase of storage modulus (G') with the excitation shear rate was controllable by varying the external magnetic field. In consideration of its plastic behavior and rate dependent characteristics, ST composite was beyound an body armor but also an ideal matrix for flexible force sensors if conductive substrate was introduced into the polymer. Carbon nanotubes, with extraordinary electrical conductivity, mechanical and low density characteristics, were ideal nanofillers to reinforce and functionalize traditional polymer materials. [38-41] To this end, the MWCNT-based ST polymer composite might be an interesting body armor with both excellent protective performance and the compression rate-dependent conductivity.

In this paper, a rate-dependent conductive shear stiffening composite with both excellent safe-guarding and force sensitive performance was developed. Firstly, MWCNT was treated by using a ethanol etching method to improve its dispersity in the polymer matrix. Then, the MWCNT hybrid shear stiffening polymer was

prepared by using a simple solution mixing method. The presence of MWCNT induced a tremendous increase in both ST performance and conductivity. The compression rate dependent conductivity was investigated and the force signals can be detected by the negative piezoresistivity effect in quasi-static compression test. Thanks to the ST effect, the polymer composite acted as a protector and absorb much energy during the impact process. Obviously, the plastic, self-healing and rate-dependent conductive MWCNT/ST-PC is promising for a novel force sensor with well defined body safe-guarding property. Finally, a possible mechanism was proposed to analyze the impact dependent sensitivity.

2. Experimental Section

2.1 Materials

Acetone and alcohol are purchasing from Sinopharm Chemical Reagent Co. Ltd, Shanghai, China. MWCNT with the diameter of 8-13 nm and length of 3-12 μm is provided by Conductive Materials of Luelida Co. Ltd, Xinxiang City, Henan province, China. Benzoyl peroxide (BPO) and sodium dodecyl benzene sulfonate (SDBS), (provided by Sinopharm Chemical Reagent Co. Ltd, Shanghai, China), are used as cross-linking agent and surfactant, respectively. The above reagents are of analytical purity before use.

2.2 One-step solution mixing method to prepare MWCNT/ST-PC

The polymer matrix used in this paper is a derivative of polyborondimethylsiloxane (PBDMS) and it was prepared according to our previous work.[37] Firstly, different amounts of MWCNT and SDBS with a weigh ratio of 5:1 were homogeneously dispersed in a 200 mL mixed solvents of alcohol and acetone (1/1, v/v) in a round-bottomed flask by stirring continuously for 2h. Then, 9.6 g of PBDMS and 0.384 g of BPO were introduced to the mixed solvents and stirred for another 1h. The suspensions were then pulled into beakers and sonicated for 14h. Finally, the slurry was dried under vacuum to remove the solvents. The resulting

solid materials were then mixed homogeneously by a two-roll mill (Taihu Rubber Machinery Inc., China, model XK-160) and vulcanized in an oven at 80 ℃ for 2h. To investigate the influence of the MWCNT, similar experiments were conducted. The pristine MWCNTs were treated by 200 mL acetone and 200 mL mixed solvents of alcohol and acetone (1/1, v/v), respectively. Other procedures were the same without adding polymer matrix and BPO.

In addition, the mass fractions of MWCNT in the matrix were kept at 0, 0.1, 0.5, 1, 2 and 3 wt%, respectively. For convenience, the composite materials with different mass fractions of MWCNT were defined as MWCNT/ST-PC-X%, where X was the contents of nanofillers. For example, the MWCNT/ST-PC-1% indicated that 1wt% MWCNT were filled in the ST-PC. The pristine MWCNT and treated MWCNT (by acetone and mixed solvents) were named as P-MWCNT, A-MWCNT and A-A-MWCNT.

2.3 Characterization

The morphology of the primary and etched MWCNT were investigated by SEM (JEOL JSM-6700F) and TEM (JEM-2011). Additionally, MWCNT/ST-PC-0.5% and MWCNT/ST-PC-1% were sliced into films with the thickness of 80 nm by cryosection system (Leica EM FC7 UC7) and the dispersion state of MWCNT were observed by TEM (JEM-2100). A rheometer (Physica MCR 301, Anton Paar Co.,Austria) was used to characterize the shear stiffening effect of MWCNT/ST-PC specimens. Samples were molded into cylinders with the thickness of 0.68 mm and the diameter of about 20mm. The shear frequency swept from 0.1 Hz to 100 Hz and the strain was set at 0.1%.

2.4 Electric conductivity testing system

The accessories of EIS system (shown in Fig.1) include modulab material test systems (a), data storage and analyzing system (b) and a teflon mould (c). As shown in the sample holder (Fig.1d), the black part denotes the test sample and the yellow parts are copper electrodes. The upper electrode is mobilizable so as to control the sizes of samples. Fig.1e was the dynamic conductivity measurement devices and the measurement parts include modulab material test systems, data storage and analyzing

system. The compression with different rates is realized by dropping the weight from different heights and it is clear that compression rate increases with the increase of falling height (Fig.1a and b). Additionally, electrical characterization included constant voltage scanning (1 V, 60 s), linear sweep I-V test and triangular sweep I-V measurement. The voltage increased from 0 V to 2 V and the current was recorded during the linear sweep I-V test. In the triangular sweep I-V characterization, the voltage varied from 0 V to 1 V and swept back to initial value and the current under different stimulus was measured.

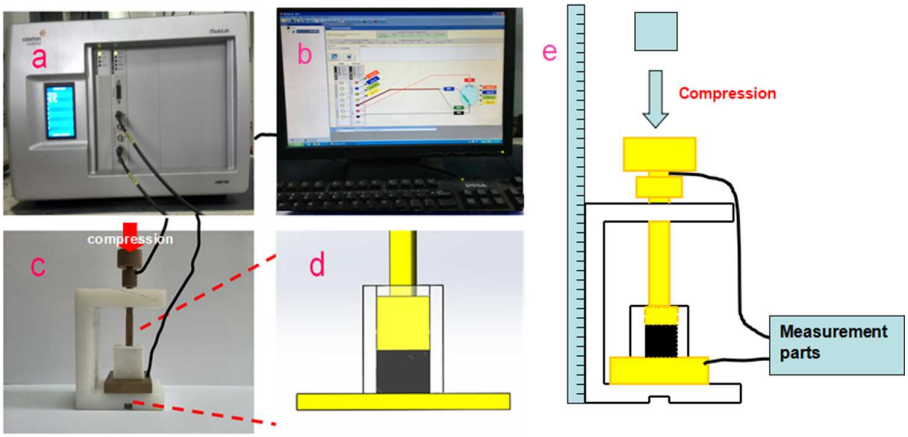

Fig.1 Schematic of (a-d) EIS measurement systems and (e) compression rate-dependent conductivity test setup.

2.5. The dynamic mechanical analysis (DMA)

Dynamic mechanical tests of the MWCNT/ST-PC-2% were performed by the dynamic mechanical analysis machine (DMA Q800) with shear pattern and Figure 2 showed the measurement systems. Samples were cut into small cubes, with 10 mm in length, width and 4 mm in thickness. The measurements were conducted at 1 and 10Hz at heating rates of 3□/min from -50 to 60 □.

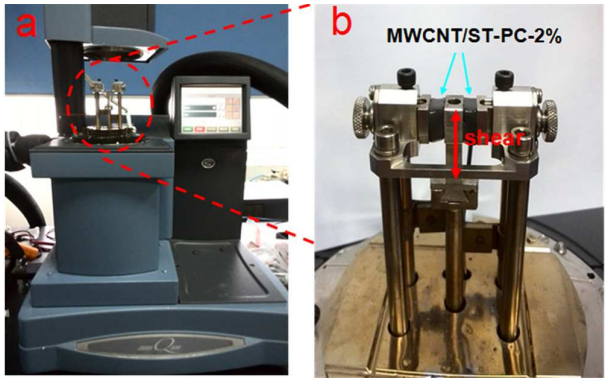

Figure 2. Schematic of DMA measurement systems

3 Results and Discussion

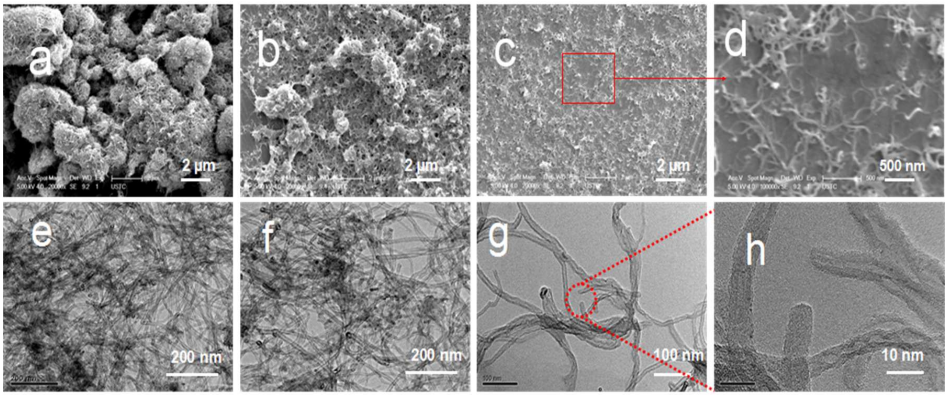

Fig.3 SEM images of (a) P-MWCNT, (b) A-MWCNT and (c and d) A-A-MWCNT. Typical TEM images of (e) P-MWCNT, (f) A-MWCNT and (g) A-A-MWCNT; HRTEM images of (h) A-A-MWCNT.

To improve the performance of the composite, the MWCNT was treated under different organic solvents.[23,42] Figure 3 shows the SEM and TEM images of the P-MWCNT (pristine), A-MWCNT (acetone) and A-A-MWCNT (mixed solvent). A large number of bundles are visible in P-MWCNT and A-MWCNT, indicating the nanotubes are aggregated and they must be very difficult to form uniform dispersion in solvent or polymer matrix. Interestingly, the A-A-MWCNT are uniformly dispersed on the copper grid and no aggregation is found in a large visual field. As shown in the high magnification TEM image, the surface of the A-A-MWCNT is relatively smooth and clean, indicating the positive performance of the solvent treating. It was reported that the solvent eching broke the nanostructure of the

MWCNT. [43, 44] In this work, the TEM image demonstrates the side walls of nanotubes were well kept after the eching treatment, thus the excellent conductivity of A-A-MWCNT could be expected. Obviously, the above results prove that the solvent etching method is a new strategy to improve the dispersity of MWCNT in polymer matrix.

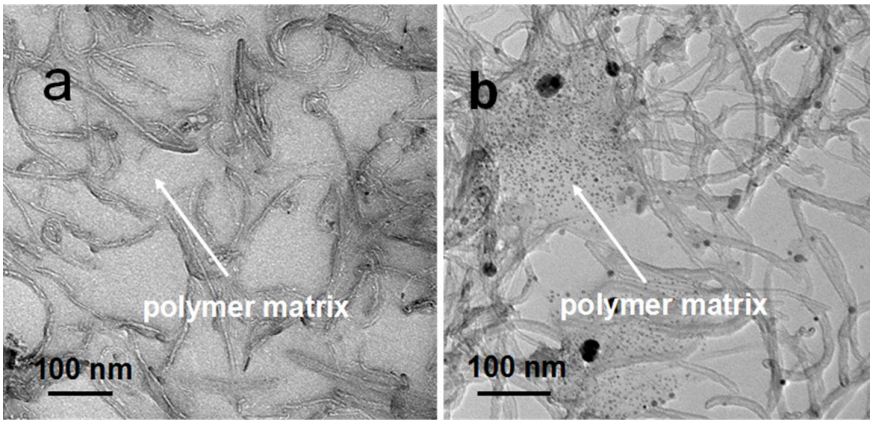

Fig.4 TEM images of MWCNT/ST-PC-0.5% and MWCNT/ST-PC-1%.

Because of the well dispersity, the MWCNT could be very easily introduced into the polymer matrix to form multifunctional nanocomposites. Fig.4a and b are the TEM images of MWCNT/ST-PC-0.5% and ST-PC/MWCNT-1% samples. It is found that the size and length of the MWCNT are similar to the treated MWCNT (Fig.3g), indicating the mix and vulcanization process performs little influence on the MWCNT. Since the high aspect ratio of pristine CNTs, random, curled structure, and large aggregates of bundles were usually observed. In this work, the length of the as-prepared MWCNT is shortened, thus the dispersion of MWCNT in polymer matrix is significantly improved. Previous work believed that the shorten length of CNT and the surrounding polymer matrix will notablely reduce the conductivity of polymer composite.[45] However, due to the homogeneous dispersion in this work, the three dimensional conductive network formed by shortened MWCNT reduces the gaps between nanotubes and leads to the formation of more effective conductive paths (ECPs), which will further improve the conductivity.[46] To this end, with increasing of the MWCNT content, the conductivity will increase.

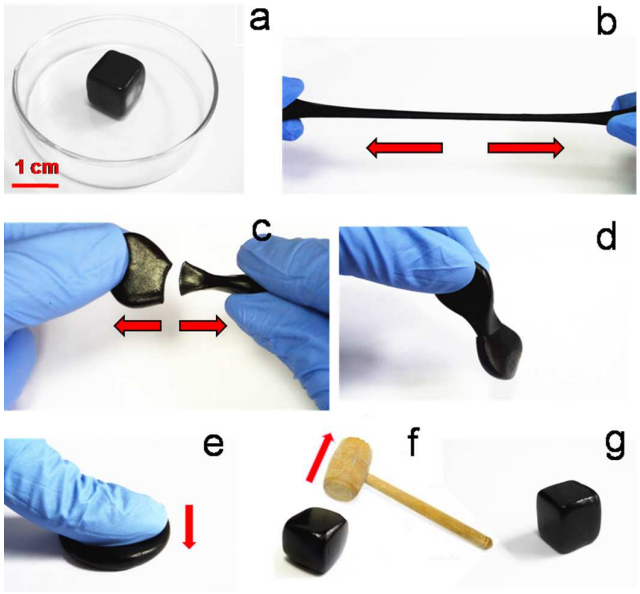

Fig.5 Deformations of MWCNT/ST-PC-2% with different external excitation: prestine sample with the dimension of 10 × 10 × 10 mm (a), strecthed slowly (b), stretched quickly (c) and self-healing (d), compressed slowly (e) and violently (f), after self-healing and kneading treatment (g).

Since the WMCNT/ST-PC presents a plastic characteristic, it is necessary to assess the flexibility and self-healing behavior of as-prepared nanocomposite. Fig.5a shows the as-prepared sample with the dimension of 10 × 10 × 10 mm. Once stretched (b) and compressed (e) slowly, the composite is ductile and can be molded into various shapes which exhibits plastic characteristic. Interestingly, if stretched quickly (Fig.5c), the composite fractures abruptly and displays solid state, presenting shear stiffening property. However, the fractured samples can heal once the two pieces touch with each other (Fig.5d). Similarly, Fig.5f shows if impacted violently, the MWCNT/ST-PC-2% is difficult to be compressed and can maintain its shapes. Finally, all the deformed samples can be self-healed and molded into prestine shapes which displays in Fig.5g.

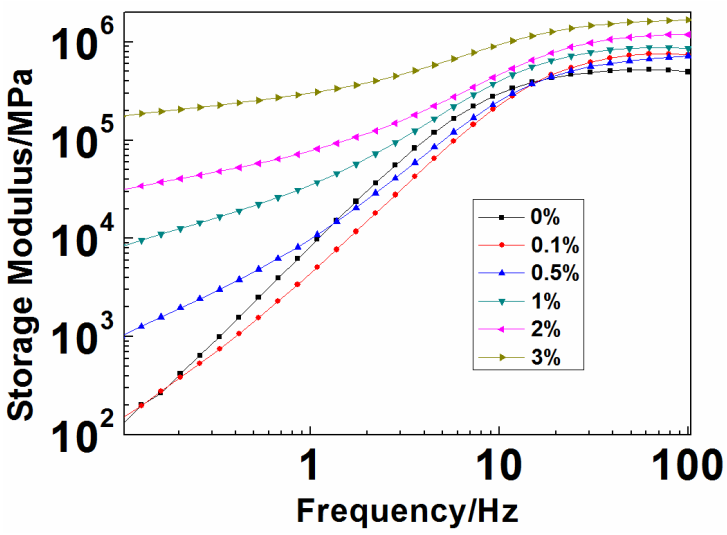

Fig. 6 Storage modulus (G') of as-prepared samples with different MWCNT contents.

Inherited from the PBDMS, the MWCNT/ST-PC pocesses excellent shear stiffening characteristics. Fig. 6 shows the frequency-dependent storage modulus (G') of MWCNT/ST-PC samples. G' of all samples increase dramatically with increasing of the excitation frequency, presenting a pronounced ST effect. When excited by shear stress with the frequency at 0.1 Hz, G'_{min} of MWCNT/ST-PC-0% is 125 Pa, which presents a plastic characteristic. As soon as the frequency increases to 100 Hz, G'_{max} reaches to 0.50 MPa, indicating a typical shear stiffening property. Moreover, content of the MWCNT exhibits a significant inflence on the mechanical properties of as prepared nanocomposites. In comparison to MWCNT/ST-PC-0%, the G'_{min} of MWCNT/ST-PC-0.5% is 0.01 MPa, indicating the MWCNT critically strengthen the polymer matrix. Similarly, with further increasing of the MWCNT content, the G'_{min} increases to 0.1, 0.2, 1 MPa, respectively. Although the G'_{max} also increases with increasing of the MWCNT content, the ST effect (the ratio of G'_{max}/G'_{min}) decreases since the sharp increasing of the G'_{min}. G'_{max} of MWCNT/ST-PC with MWCNT contents of 0%, 0.5%, 1%, 2% and 3% are 0.50, 0.72, 0.87, 1.19, and 1.69 MPa and the ST effects are 396720%, 70590%, 10460%, 3967% and 939%, respectively. Therefore, proper MWCNT content is desired for its unique application in the relative practice. Based on the above analysis, it is concluded that the ST-PC specimens

exhibit typical shear stiffening characteristic under shear stress with different rates, thus they can act as a novel kind of flexible protective material. The tremendous reinforcement in ST effect is attributed to the homogeneous dispersion of MWCNT and the strong interfacial adhesion between polymer chains and MWCNT.

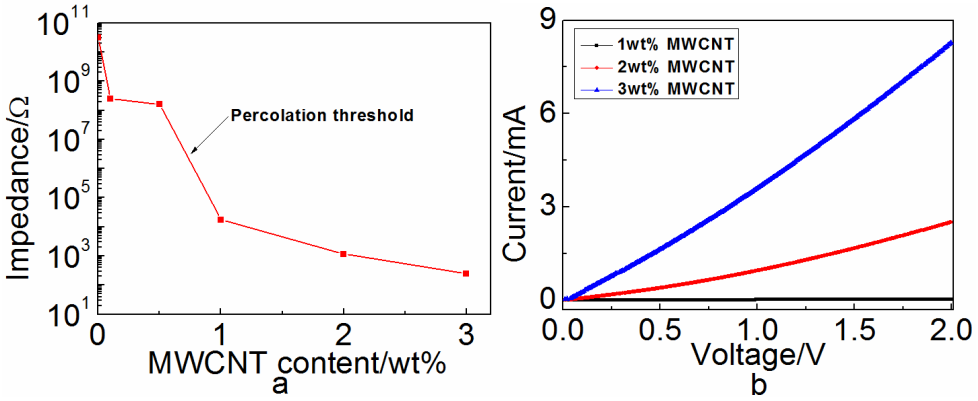

Fig.7 Results of electrical properties of (a) impedance as a function of MWCNT content and (b) I-V curves.

EIS is applied to study the electrical performance of MWCNT based ST-PC (Fig.7). In the impedance measurement, the scanning frequency is set at 1 Hz and the impedance (Z) as a function of MWCNT mass fraction is presented in Fig. 7a. It is observed that the impedance of samples decrease with the increase of MWCNT content and Z of MWCNT/ST-PC-0.5% and MWCNT/ST-PC-1% are 1.62×10^8 Ω and 1.76×10^4 Ω respectively, which indicates the percolation threshold is between 0.5% and 1%. Fig.7b reveals a linear relationship between current and voltage of specimens. A decrease trend in resistance is observed and it is in accordance with impedance test results. Meanwhile, it is calculated from the linear I-V curves that the resistivity of MWCNT/ST-PC-1%, MWCNT/ST-PC-2% and MWCNT/ST-PC-3% are 1.3×10^3, 10.2 and 2.1 Ω m, respectively. Consequently, it is highlighted that the enhancement in conductivity by low content of etched MWCNT is remarkable.

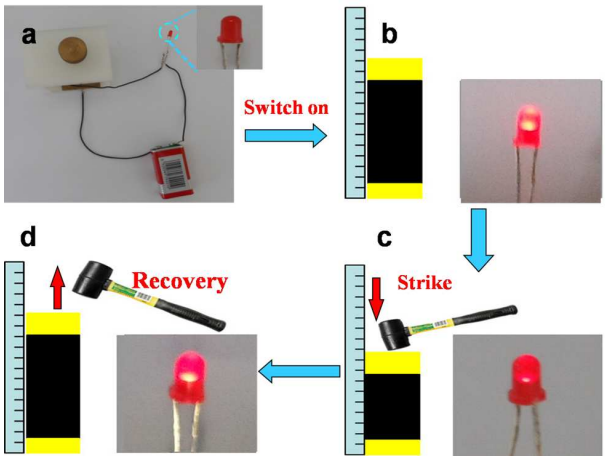

Fig.8 Photographs of pressure response of MWCNT/ST-PC by resistivity variation.

Due to its critical shear stiffening nature, the impedance of the nanocomposite also exhibits a impact rate-dependent characteristic. To qualitatively illustrate the response of pressure, a schematic testing system is displayed in Fig.8. A circuit, composed of a cell, a LED bulb and the conductive polymer composite held by the Teflon mould, is observed in Fig.8a. Particularly, the light intensity of bulb is significantly reduced as soon as a hammer is stroke on the upper copper electrode. This phenomenon suggests the electrical resistance of polymer composite is dramatically increased when the composite is impacted with high rate (Fig. 8c and d). Then, the polymer composite is taken out and kneaded. Interestingly, it is found that the light intensity recovers, indicating that the resistance decreases to initial value after the healing treatment (Fig. 8e). To this end, we can conclude that the resistance of ST-PC specimens is strongly dependent on the compression rate and high-rate impact will induce the polymer composite from conductor to insulator.

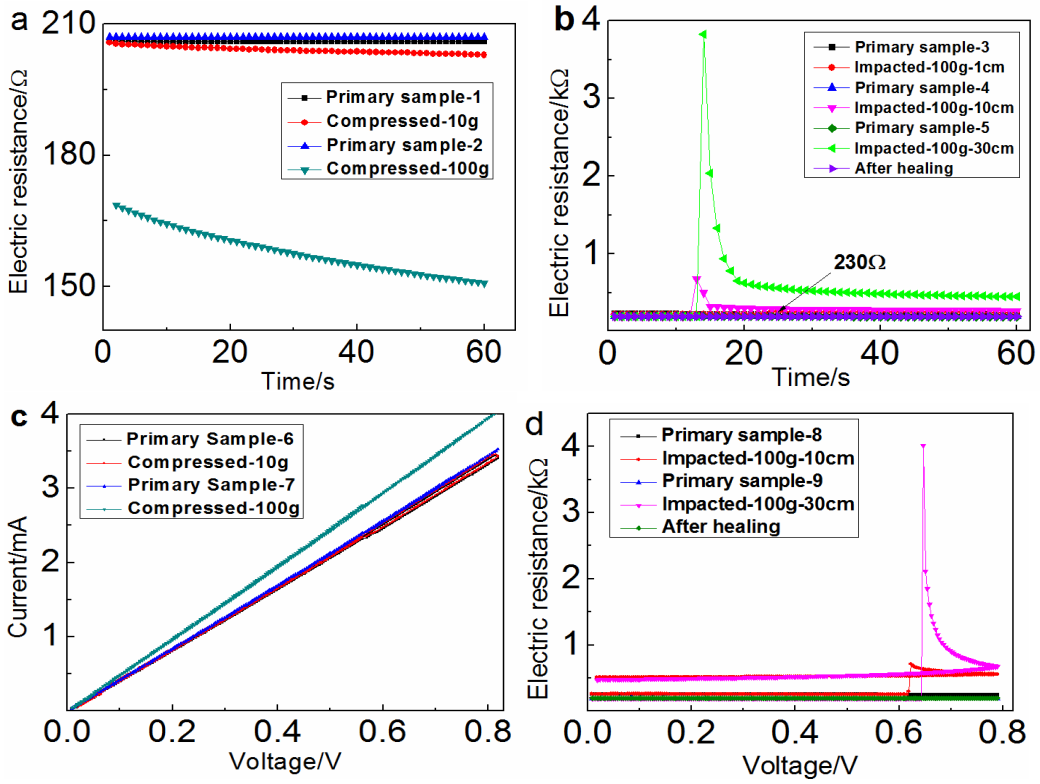

Fig.9 Characterizations of the resistive pressure response of MWCNT/ST-PC. Linear sweep R-t curves of (a) : quasi-statical compression and (b) : dynamic compression; triangular sweep R-t curves of (c) : statical compression and (d) : dynamic compression.

To investigate the quasi-statical conductivity of MWCNT/ST-PC stimulated by compression with different rates, 9 MWCNT/ST-PC-2% specimens with the shape of 10 × 10 × 10 mm are prepared and placed in the compressible mould (Fig.1e). In Fig.8a and b, samples are loaded under a constant voltage (1 V) and R-t curves under different quasi-statical mass loading (10 g and 100 g respectively) are recorded. Obviously, resistance of the samples loaded with pressure is decreased and the decreasing level is more obvious with the increase of pressure. (Fig.9a) This pressure dependence of reduced resistance effect is named as piezoresistance effect. It is mainly because under quasi-static compression (low rate), the gaps between nanotubes are decreased and more effective conductive paths are formed, leading to

the reduction in resistance. Therefore, the decrease in resistance can reflect the loaded pressure in quasi-statical mass loading conditions.

In the high rate compression test, a 100 g weight falls down from 1 cm, 10 cm and 30 cm to excite the samples and R-t curves are presented in Fig. 9b. Conversely, Resistivity of specimens increase sharply under the instantaneous impact. For instance, it is calculated that the resistivity of primary sample-3 increases from 1.90Ω m to 2.30 Ω m after impacted by 100g weight falling from 1 cm. In addition, the resistivity of primary sample-5 changes from 1.92 Ω m to 38.29 Ω m after impacted from 30 cm and finally attenuates to 4.50 Ω m, indicating that the polymer absorbs much energy and the microstructures are dramatically changed after impact. Then, the composite is took out of the mould and kneaded. It is then found that the resistivity recoveries to the initial value. Similarly, primary sample-4 exhibits the same characteristic and maximum resistivity of the impacted sample-4 is 5.38 Ω m, which is lower than 38.29 Ω m. Therefore, the composite exhibits pressure-dependent conductivity and the sensitivity is also very high.

Fig.9c and d show the triangular sweep R-t curves and the loaded voltage varies from 0 V to 0.81 V and then decreases to initial value. Compared with the results shown in Fig.9a and b, the changes in resistance behave the same trend. Additionally, the resistance keeps constant after relaxation and they are all larger than the initial data. However, owing to the plasticity, the resistance could recover to initial value easily after healing treatment. To this end, it is concluded the conductivity shows strongly pressure dependent characteristic and MWCNT/ST-PC with tunable conductivity and protective performance is appropriate to prepare novel force sensors and protect human beings.

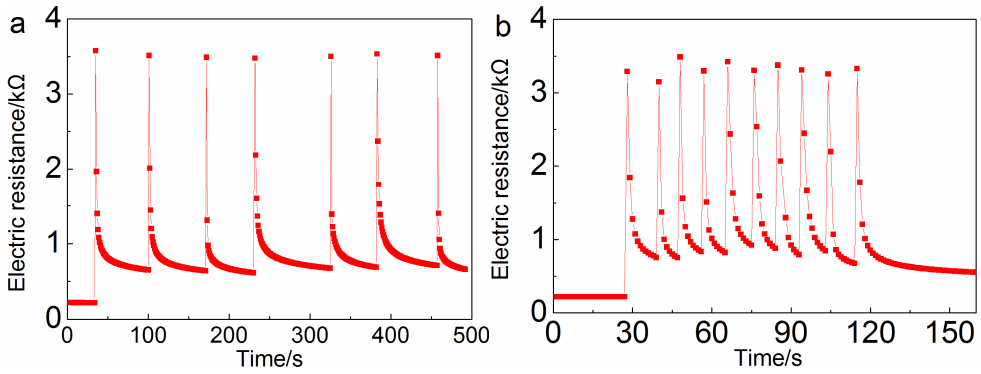

Fig.10 Cycle stability of mechanical and electrical performance of MWCNT/ST-PC-2% by the impact of a 100 g weight falling from 30 cm with (a) and without (b) relaxation.

Since cycling stability was very significant for practical application, it is essential to evaluate the reproducibility of mechanical and electrical performance under consetitive excitation. Fig.10a and b present the plot of electrical resistance versus time under the excitation of a 100 g weight falling from 30 cm by repeated cycles and the interval between consecutive impact are 60 s (with relaxation) and less 10 s (without relaxation) which are aimed to simulate practical continuous impacts. In Fig.10a, the resistance increased sharply from 220 to 3668 Ω as soon as impacted and subsequently relaxed to 672 Ω within 60 s. Remarkably, we demonstrated the degradation of resistance in the subsequent cyclic stability test is slight, indicating the as-prepared nanocomposite could remain steady in mechanical and electrical behaviors with relaxation. Additionally, the electrical performance could still be highly stable and the response to external over multiple cycles of impact is ideal without relaxation (less than 10 s) as shown in Fig.10b. Therefore, the results provided direct evidence that the as-prepared nanocomposite can recover its performance quickly and the excellent cyclic stability is beneficial for practial shock application.

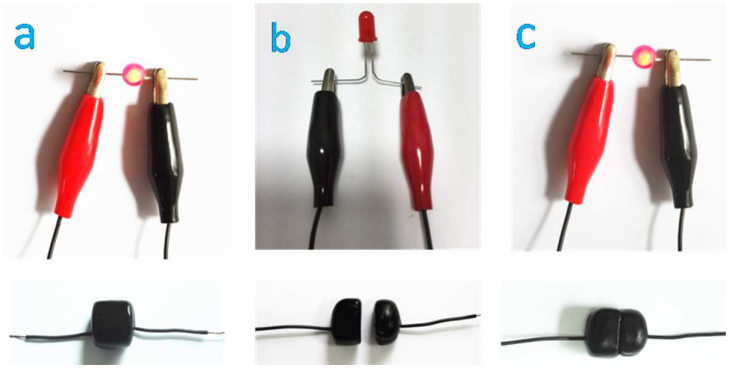

Fig.11 Self-healing electrical conductivity of the asprepared nanocomposite: (a) Original undamaged sample, (b) after cutting (c) contact and healing.

Since self-healing property is very sigficant for practical application,[47] it is essencial to access the self-healing electrical conductivity of the asprepared nanocomposite and a LED bulb was applied to monitor the changes of conductivity in a tandem circuit. As shown in Fig11a, the LED bulb lights up brightly at a voltage of 9 V. However, after cutting the as-prepared MWCNT/ST-PUC-2% into two pieces, it is without doubt that the LED extinguishes immediately (Fig.11b). Interestingly, as soon as the two pieces are touched with other (Fig.11c), the LED lights up again and the brightless are almost the same as before self-healing, indicating the changes of the resistance is negligible. Therefore, this process demonstrate this novel shear stiffening nanocomposite can exhibite excellent self-healing property at room temperature.

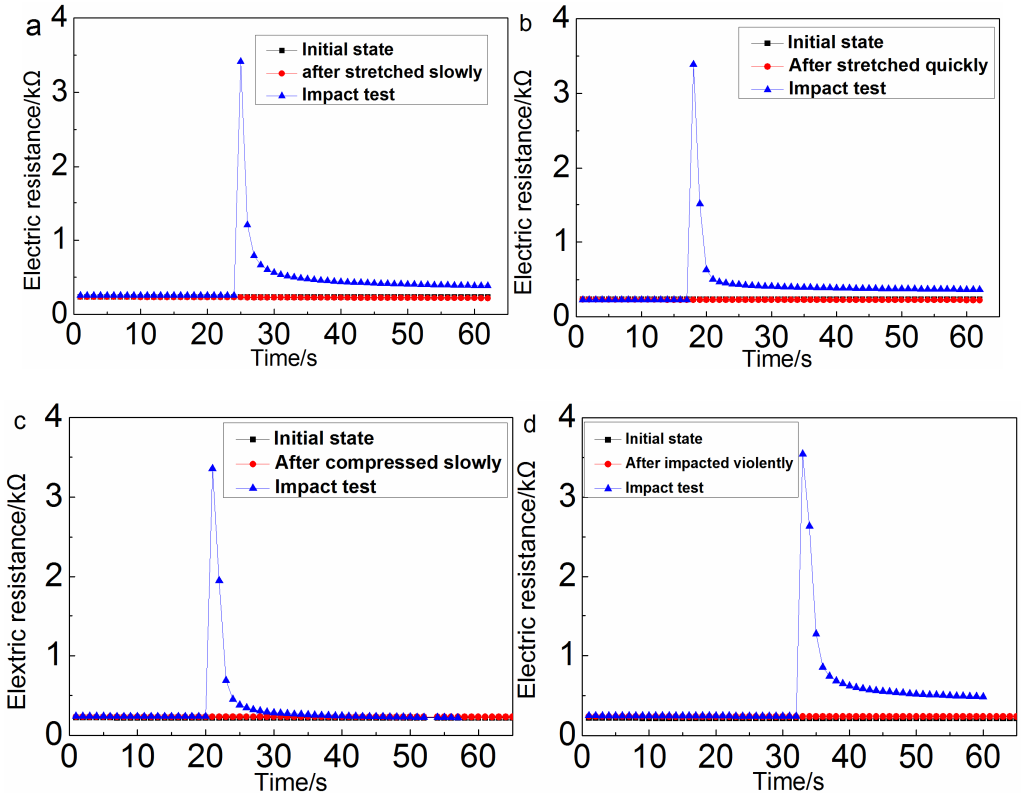

Fig.12 Changes of electrical properties of MWCNT/ST-PUC before and after various deformations: stretched slowly (a) and quickly (b), impacted slowly (c) and violently (d).

Fig.12 shows the changes of electrical performance before and after various exictations which is aimed to estimate the performance stability. In Fig.12a, the initial electrical resistance of MWCNT/ST-PC-2% is 223 Ω. Particularly，after stretched slowly and self-healed (shown in Fig.5b and g), the resistance recover to 229 Ω and if impacted by a 100 g weight falling from 30 cm, the highest response of electrical resistance is 3495 Ω，which is parallel to those in Fig.9b, exhibiting stable performance. Analogously, the electrical properties can also be well maintained after the composite is self-healed from other deformations, such as stretching (Fig.5c) or compression (Fig.5e and f), suggesting the reliability after self-healing treatment.

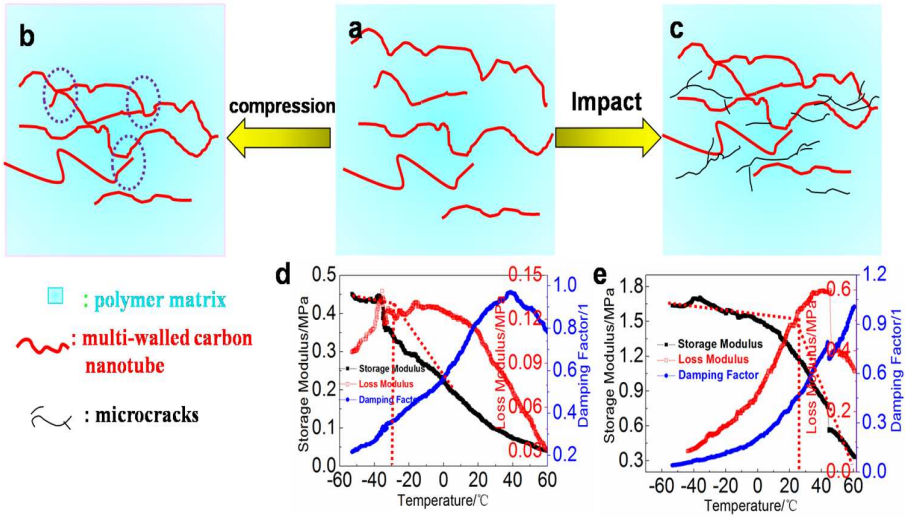

Fig.13 (a-c): Microstructure changes induced by different compression rates, Dynamic mechanical tests of MWCNT/ST-PC-2% at (d):1Hz and (e) 10 Hz.

Glass transition phenomenon, known as polymer transfers from rubbery state to glassy state, is attributed to the movements of different polymer chains.[48,49] Clearly, glass transition temperature (Tg) can increase with increasing measurement temperature or decreasing stimuli frequency.[50] Previously, we found that the polymer matrix play a dominated role for the shear stiffening characteristics.[37] The O atom can share electrons with the empty p orbit of B atom and the shared electrons are called "B-O cross bonds". The "cross bonds" are transient, dynamically variable and much more vulnerable than covalent bonds. Therefore, the B-O bond opens and relaxes easily if stimulated by a stress with low rate and the deformation and movement of polymer chains is easy. Therefore, when the shear frequency is 1 Hz, Tg is – 30 □. However, when stimulated by shear stress with 10 Hz (Figure 13d), the B-O bonds cannot adjust themselves to adapt the external stimuli because of their longer relaxation time. In this case, the large number of the cross bonds may seriously impede the movement of entangled molecular chains. Under this circumstance, Tg shifts to 27 □. (Figure 13e) Since the rheological and electrical measurements are conducted at 25 □, thus, when stimulated by 1Hz, MWCNT/ST-PC-2% is in rubber state and G'_{min} is 0.03MPa, presenting plastic characteristic. Similarly, when the shear

frequency increases to 10Hz, the nanocomposite is in glassy state and G'_{min} increases to 1.19 MPa, exhibiting excellent ST performance.

Here, the conductivity is also rate dependent. In statical compression (low rate) condition, the composite is plastic. During the loading process, the polymer composite is condensed and the distance between adjacent carbon nanotubes decreases. When the gaps between nanotubes are small enough, the tunneling effects occur. More effective conductive paths (ECPs) are formed, thus the resistance decreases (Figure 13b). Nevertheless, two kinds of microstructural changes exist in the impact process (high rate). Firstly, the impact will reduce the gaps of nanotubes which will form more ECPs and the resistance reduces. Instantaneously, under an external applied impact, the storage modulus of MWCNT/ST-PC sharply increased thus it transform from plastic to solid-like state. To absorb the impacting energy, a number of crazing appears in solid materials. These microcracks seriously separate the contacted MWCNTs and destroy the ECPs, thus the resistance sharply increases (Figure 13c). Apparently, the destruction effect is dominant in the impact process. Therefore, the microstructures of ECPs are destroyed and the resistance increases. After kneaded, the microcracks are healed and resistance reduces to the initial value. Therefore, this compression rate dependent resistance characteristic enable the nanocomposite be widely applied in the force sensors.

5. Conclusion

In this work, a rate-dependent conductive shear stiffening composite with both excellent safe-guarding and force sensitive performance was developed. Here, the solvent aching was employed to treat the MWCNT thus they can uniformly dispersed into the polymer matrix. The prepared nanocomposites exhibited typical shear stiffening characteristic and their storage modulus obviously increased with the increasing of excitation frequency. EIS method were applied to study the electrical properties of polymer/CNT composite and revealed the percolation threshold was between 0.5% and 1wt%. Under statical compression, the resistance decreased with increasing of the pressure. However, the conductivity sharply decreased once the

compression rate quickly increased. The mechanism of ST effect and the compression rate dependent conductivity were presented. It is believed the interaction of B-O cross bond induces the shear stiffening effect and the conduction behaviors under compression with different rates. On account of the protection effect, plasticity and tunable conductivity, the novel polymer/CNT composite can be potentially applied as force sensitive body armor.

Acknowledgments

Financial supports from the National Natural Science Foundation of China (Grant Nos. 11372301, 11125210), Anhui Provincial Natural Science Foundation of China (1408085QA17) and the National Basic Research Program of China (973 Program, Grant No. 2012CB937500) are gratefully acknowledged. This work was also supported by Collaborative Innovation Center of Suzhou Nano Science and Technology.

References

[1] B. Karamis, A. Cerit and F. Nair, *J. Compos. Mater.,* 2008, **42,** 2483.

[2] G. M. Zhang, R. C. Batra and J. Zheng, *Compos. Part. B: Eng.,* 2008, **39,** 476.

[3] P. Tan, *Mater. Design.,* 2014, **64,** 25.

[4] S. Feli and M. R. Asgari, *Compos. Part. B: Eng.,* 2011, **42,** 771.

[5] S. E. Atanasov, C. J. Oldham, K. A. Slusarski, J. T. Scarff, S. A. Sherman, K. J. Senecal, S. F. Filocamo, Q. P. McAllister, E. D. Wetzel and G. N. Parsons, *J. Mater. Chem. A.,* 2014, **2,** 17371.

[6] L. B. Tan, K. M. Tse, H. P. Lee, V. B. C. Tan and S. P. Lim, *Int. J. Impact. Eng.,* 2012, **50,** 99.

[7] Y. Zhou, X. G. Chen and G. Wells, *Compos. Part. B: Eng.,* 2014, **62,** 198.

[8] T. N. Ng, W. S. Wong, M. L. Chabinyc, S. Sambandan, R. A. Street, *Appl. Phys. Lett.,* 2008, **21,** 213303.

[9] Y. K. Fuh, J. C. Ye, P. C. Chen and Z. M. Huang, *J. Mater. Chem. A*, 2014, **2**, 16101.

[10] H. Deng, M. Z. Ji, D. X. Yan, S. R. Fu, L. Y. Duan, M. W. Zhang and Q. Fu. *J. Mater. Chem. A.*, 2014, **2**, 10048.

[11] C. Y. Pang, G. Y. Lee, T. Kim, S. M. Kim. H. N. Kim, S. H. Ahn and K. Y. Suh, *Nat. Mater.,* 2012, **11,** 795.

[12] J. S. Chun, K. Y. Lee, C. Y. Kang, M. W. Kim, S. W. Kim and J. M. Baik, *Adv. Funct. Mater.,* 2014, **24,** 2038.

[13] C. Q. Ye, M. Z. Li, M. Q. Xue, W. Z. Shen, T. B. Cao, Y. L. Song and L. Jiang, *J. Mater. Chem.,* 2011, **21,** 5234.

[14] K. Noda, K. Matsumoto and I. Shimoyama, *Sensor. Actuat. A.,* 2014, **215,** 123.

[15] C. L. Choong, M. B. Shim, B. S. Lee, S. Jeon, D. S. Ko, T. H. Kang, J. Bae, S. H. Lee, K. E. Byun, J. Im, Y. J. Jeong, C. E. Park, J. J. Park and U. I. Chung, *Adv. Mater.,* 2014, **26,** 3451.

[16] Y. Hou, D. R. Wang, X. M. Zhang, H. Zhao, J. W. Zha and Z. M. Dang, *J. Mater. Chem. C.,* 2013, **1,** 515.

[17] J. H. Hwang, J. Jang, K. Hong, K. N. Kim, J. H. Han, K. Shin and C. E. Park, *Carbon.,* 2011, **49,** 106.

[18] W. L. Hu, X. F. Niu, R. Zhao and Q. B. Pei, *Appl. Phys. Lett.,* 2013, **102,** 083303.

[19] S. Mannsfeld, B. Tee, R. Stoltenberg, C. Chen, S. Barman; B. Muir, A. Sokolov, C. Reese and Z. N. Bao, *Nat. Mater.,* 2010, **9,** 859.

[20] A. V. Shirinov and W. K. Schomburg, *Sensor. Actuat. A.,* 2008, **142,** 48.

[21] B. Sun; Y. Long, Z. J. Chen, S. L. Liu, H. D. Zhang, J. C. Zhang and W. P. Han, *J. Mater. Chem. C.,* 2014, **2,** 1209.

[22] S. Yun, S. Park, B. Park, Y. S. Kim, S. K. Park, S. Nam and K. U. Kyung, *Adv. Mater.,* 2014, **26,** 4474.

[23] M. T. Byrne and Y. K. Gunko, *Adv. Mater.,* 2010, **22,** 1672.

[24] S. Li, Z. P. Guo, C. Y. Wang, G. G. Wallace and H. K. Liu, *J. Mater. Chem. A.,* 2013, **1,** 14460.

[25] M. L. Hammock, A. Chortos, B. Tee, J. Tok and Z. N. Bao, *Adv. Mater.,* 2013, **25,** 5997.

[26] I. Clausen and T. Glott, *Sensors.,* 2014, **14,** 17686.

[27] P. Roriz, O. Frazão, A. B. Lobo-Ribeiro, J. L. Santos and J. A. Simões, *J. Biomed. Opt.,* 2013, **18,** 050903.

[28] N. T. Tien, S. H. Jeon, D. I. Kim, T. Q. Trung, M. Jang, B. U. Hwang, K. Eun. Byun, J. Bae, E. Lee, J. Tok, Z. N. Bao, N. E. Lee and J. J. Park, *Adv. Mater.,* 2014, **26,** 796.

[29] C. Y. Hou, H. Z. Wang, Q. H. Zhang, Y. G. Li and M. F. Zhu, *Adv. Mater.,* 2014, **26,** 5018.

[30] S. Han and Y. Y. Zhu, *Nanoscale.* 2014, **6,** 2345.

[31] F. Ye, W. Zhu, W. Q. Jiang, Z. Y. Wang, Q. Chen, X. L. Gong and S. H. Xuan, *J. Nanopart. Res.,* 2013, **15,** 2122.

[32] T. F. Tian, W. H. Li, J. Ding, G. Alice and H. P. Du, *Smart. Mater. Struct.,* 2012, **21,** 125009.

[33] X. Z. Zhang, W. H. Li and X. L. Gong, *Smart. Mater. Struct.,* 2008, **17,** 035027.

[34] C. Neagu, P. E. Bourban and J. A. Manson, *Compos. Sci. Technol.,* 2009, **69,** 515.

[35] X. L. Gong, Y. L. Xu, Wei. Zhu, S. H. Xuan, W. F. Jiang and W. Q. Jiang, *J. Compos. Mater.,* 2014, **48,** 641.

[36] P. Green, R. Palmer. U.S. Patent 2010/0132099 A1, 2010.

[37] S. Wang, W. Q. Jiang, We. F. Jiang, F. Ye, Y. Mao, S. H. Xuan and X. L. Gong, *J. Mater. Chem. C.,* 2014, **2,** 7133.

[38] A. Lekawa-Raus, J Patmore, L. Kurzepa, J. Bulmer and K. Koziol, *Adv. Funct. Mater.,* 2014, **24,** 3661.

[39] X. M. Sun, Z. T. Zhang, X. Lu, G. Z. Guan, H. P. Li and H. S. Peng, *Angew. Chem. Int. Edit.,* 2013, **52,** 7776.

[40] D. Wang, H. Y. Li, M. F. Li, H. Q. Jiang and M. Xia, Z. Zhou, *J. Mater. Chem. C.,* 2013, **1,** 2744.

[41] A. D. Franklin, *Nature.* 2013, **498,** 443.

[42] O. V. Kharissova, B. I. Kharisov and E. G. De. Ortiz, *RCS Advances.* 2013, **3,** 24812.

[43] H. Li, J. C. Nie, J. C. Li and K. M. Sandor, *Carbon.* 2013, **54,** 495.

[44] H. Li, J. C. Li, D. Liu. P. L. Beata and K. M. Sandor, *Chem. Phys. Lett.,* 2014,**597,** 36.

[45] X. Wang, Q. Jiang, W. Z. Xu, W. Cai, Y. Inoue and Y. T. Zhu, Carbon, 2013, 53, 145-152.

[46] L. H. Wang, X. T. Wang, Y. L. Li. *Compo. Part. A: Appl. S.,* 2012, **43,** 268.

[47] S. Bubel, M. S. Menyo, T. E. Mates, J. H. Waite, M. L. Chabinyc, *Adv. Mater.,* 2015, **21,** 3331.

[48] D. Tönnies, R. Maaß and C. A. Volkert, *Adv. Mater.,* 2014, **26,** 5715.

[49] Y. Y. Wang, P. Y. Boukany, S. Q. Wang and X. R. Wang, *Phys. Rev. Lett.,* 2007, **99,** 237801.

[50] Q. Yuan, W. Jiang, L. J. An and R. K. Y. Li, Poly. *Adv. Technol.,* 2004, **15,** 409.